Facile Fabrication of Ultrafine Palladium Nanoparticles with Size- and Location-Control in Click-Based Porous Organic Polymers

Liuyi Li, Huaixia Zhao, Jinyun Wang, and Ruihu Wang*

State Key Laboratory of Structural Chemistry, Fujian Institute of Research on the Structure of Matter, Chinese Academy of Sciences, 350002, Fuzhou, Fujian China

ABSTRACT Two click-based porous organic polymers (CPP-1 and CPP-2) are readily synthesized through a click reaction. Using CPP-1 and CPP-2 as supports, palladium nanoparticles (NPs) with uniform and dual distributions were prepared through H_2 and $NaBH_4$ reduction routes, respectively. Ultrafine palladium NPs are effectively immobilized in the interior cavities of polymers. The coordination of 1,2,3-triazolyl to palladium and the confinement effect of polymers on palladium NPs are verified by solid-state ^{13}C NMR and IR spectra, XPS analyses, EDX mapping, and computational calculation. The steric and electronic properties of polymers have a considerable influence on the interaction between polymers and palladium NPs, as well as the catalytic performances of NPs. The ultrafine palladium NPs with uniform distribution exhibit superior stability and recyclability over palladium NPs with dual distributions and palladium on charcoal in the hydrogenation of nitroarenes, and no obvious agglomeration and loss of catalytic activity were observed after recycling several times. The excellent performances mainly result from synergetic effects between palladium NPs and polymers.

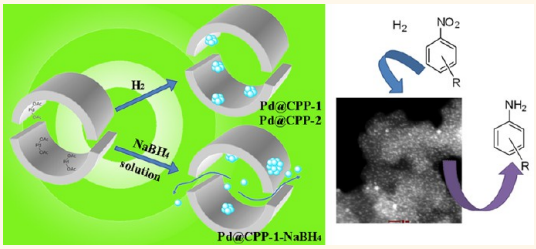

KEYWORDS: porous organic polymers · click reaction · palladium · nanoparticles · heterogeneous catalysis

The synthesis of supported metal nanoparticles (NPs) for heterogeneous catalysis has received great attention because of their unique catalytic properties and wide-ranging applicability.[1,2] The size, distribution, and morphologies of NPs as well as the property of supports have important effects on the catalytic performance.[3] Generally, small particle size may result in a high surface-to-volume ratio and provide a large number of available active sites per unit area for reaction substrates. In this context, ultrafine metal NPs are thought to be more reactive in catalysis than their bulk metal counterparts.[4−7] However, metal NPs with ultrafine size are prone to aggregate during catalytic reactions owing to their high surface energy, causing the loss of catalytic activity and recyclability.[8] To avoid the aggregation of NPs, much effort has been devoted to the enhancement of the confinement effect of the support and the interactions between the support and metal NPs.[9,10]

Recently, the fusion of porous materials and NP technology has been a fruitful area of interdisciplinary research.[11] Porous materials with high surface area and large pore volume can provide spatial confinement to prevent metal NPs from aggregating, and their channels may favor mass transfer, which are beneficial for efficient catalysis.[12,13] Immobilization of ultrafine metal NPs inside the pores of metal−organic frameworks (MOFs) has been achieved,[14,15] and superior catalytic activities and selectivities were observed.[16−18] Although MOFs with different pores and cavities can be readily modified to serve as an ideal platform for catalytically active particles,[19,20] the labile nature of the metal−ligand bonds in MOFs renders them unstable under liquid-phase catalytic conditions, which limits their extensive application in catalysis.[21] In contrast with MOFs, porous organic polymers (POPs) feature relatively stable covalent bonds[22,23] and exhibit promising applications in gas storage and catalysis.[24−28] Thanks to the state-of-the-art of molecular design of constituent monomers,[29,30] coordination groups of metal precursors or NPs can be easily introduced into

* Address correspondence to ruihu@fjirsm.ac.cn.

Received for review April 4, 2014 and accepted April 28, 2014.

Published online April 28, 2014
10.1021/nn501853g

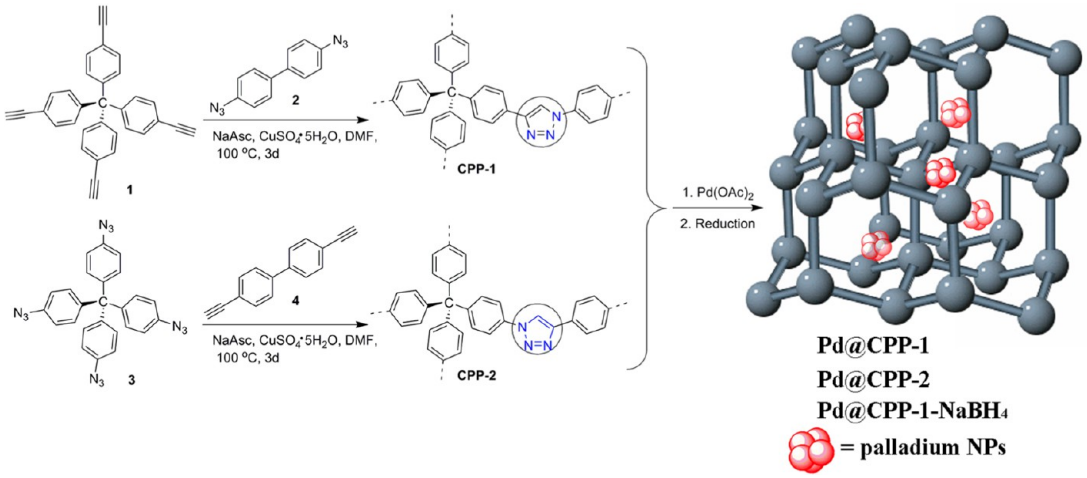

Scheme 1. Synthesis of CPP-1 and CPP-2 and the schematic illustration of Pd@CPP.

POPs to enhance the interaction between the polymers and metal precursors or particles.[31] More importantly, the properties of POPs and NPs can be facilely tuned and modified by modular synthesis and judicial selection of monomers. Thus, the optimal balance between the activity and stability of metal NPs can be achieved.[32] Very recently, POPs have been utilized as supports of metal NPs[33−40] in oxidation reactions, photocatalysis, and Suzuki−Miyaura cross-coupling reactions. However, NPs were either dispersed on the external surface of polymers or located both on the external surface and in interior pores with dual particle size distributions. The nonuniform distribution of metal active sites makes it difficult to investigate the relationships among supports, NPs, and catalytic performances.[41] Although the size control of the NPs in POPs was realized by electron reduction,[38] it is still imperative to develop a general and facile method to prepare ultrafine metal NPs inside the interior pores of POPs with a uniform distribution.

The click reaction of organic azides and terminal alkynes has attracted considerable interest owing to its superior reliability and mild reaction conditions.[42,43] The resultant 1,4-substituted 1,2,3-triazolyl efficiently serves as a connecting unit for various functional entities[44] as well as a metal-coordinating group.[45−48] Its steric and electric properties can be tuned and modified by selection of readily available terminal alkyne- and azide-containing compounds.[48] However, most click-based POPs are applied in gas sorption;[49−52] their use as supports of metal NPs for heterogeneous catalysis is extremely rare. Due to our continuing interest in the controllable synthesis of palladium NPs,[53,54] herein, we report the preparation of ultrafine palladium NPs with uniform distribution using two click-based POPs (CPP-1 and CPP-2) as supports. In comparison with palladium NPs with dual distributions and palladium on charcoal, no obvious agglomeration and loss of catalytic activity were observed after recycling several times for ultrafine palladium NPs with a uniform distribution.

RESULTS AND DISCUSSION

Following the synthetic route outlined in Scheme 1, CPP-1 was readily prepared by click reaction of tetrakis-(4-ethynylphenyl)methane with 4,4′-diazidobiphenyl in the presence of copper sulfate and sodium ascorbate, while the treatment of tetrakis(4-azidophenyl)-methane with 4,4′-diethynylbiphenyl resulted in the formation of CPP-2. In CPP-1, the tetraphenylmethane group is at the C4 postion of the 1,2,3-triazolyl ring, while it is at the N1 position in CPP-2. Both polymers are insoluble in water and common organic solvents. Elemental analyses of CPP-1 and CPP-2 show that the experimental values of C and N are slightly lower than the corresponding theoretical values. These deviations mainly result from the presence of the trapped guest molecules, which is common in porous materials. The presence of guest molecules was further supported by TGA. The weight losses of 4% and 1% before 100 °C were observed in CPP-1 and CPP-2, respectively (Figure S1).

In the IR spectra of CPP-1 and CPP-2 (Figure S2), the formation of the 1,2,3-triazolyl linkage is clearly confirmed by the disappearance of characteristic peaks of the terminal alkynyl group at 2108 and 3281 cm^{-1} and the concomitant emergence of characteristic peaks of the triazolyl group at 1618 and 3133 cm^{-1}. Solid-state ^{13}C NMR further confirms the presence of 1,2,3-triazolyl with a resonance of the C4-triazolyl carbon at 149 ppm (Figure 1). The broad signals at 110−140 ppm are attributed to aromatic carbon atoms. The characteristic peak at 64 ppm corresponds to the central carbon of the tetraphenylmethane core, which is consistent with previous analogous reports.[49,51] As shown in Figure 2, their X-ray photoelectron spectroscopy (XPS) spectra possess three peaks centered at 284.6, 399.9, and 532.2 eV, corresponding to C 1s, N 1s, and O 1s,

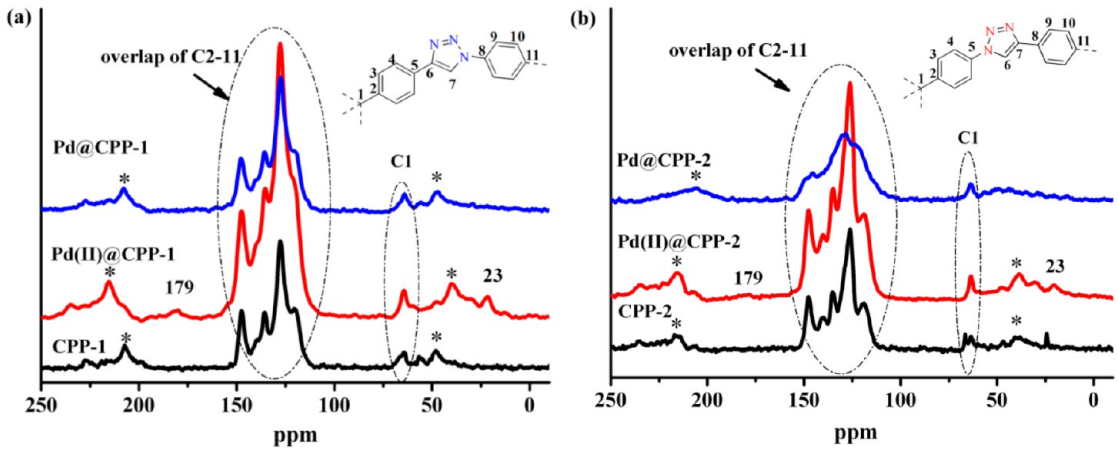

Figure 1. Solid-state ^{13}C NMR spectra for (a) CPP-1, Pd(II)@CPP-1, and Pd@CPP-1; (b) CPP-2, Pd(II)@CPP-2, and Pd@CPP-2.

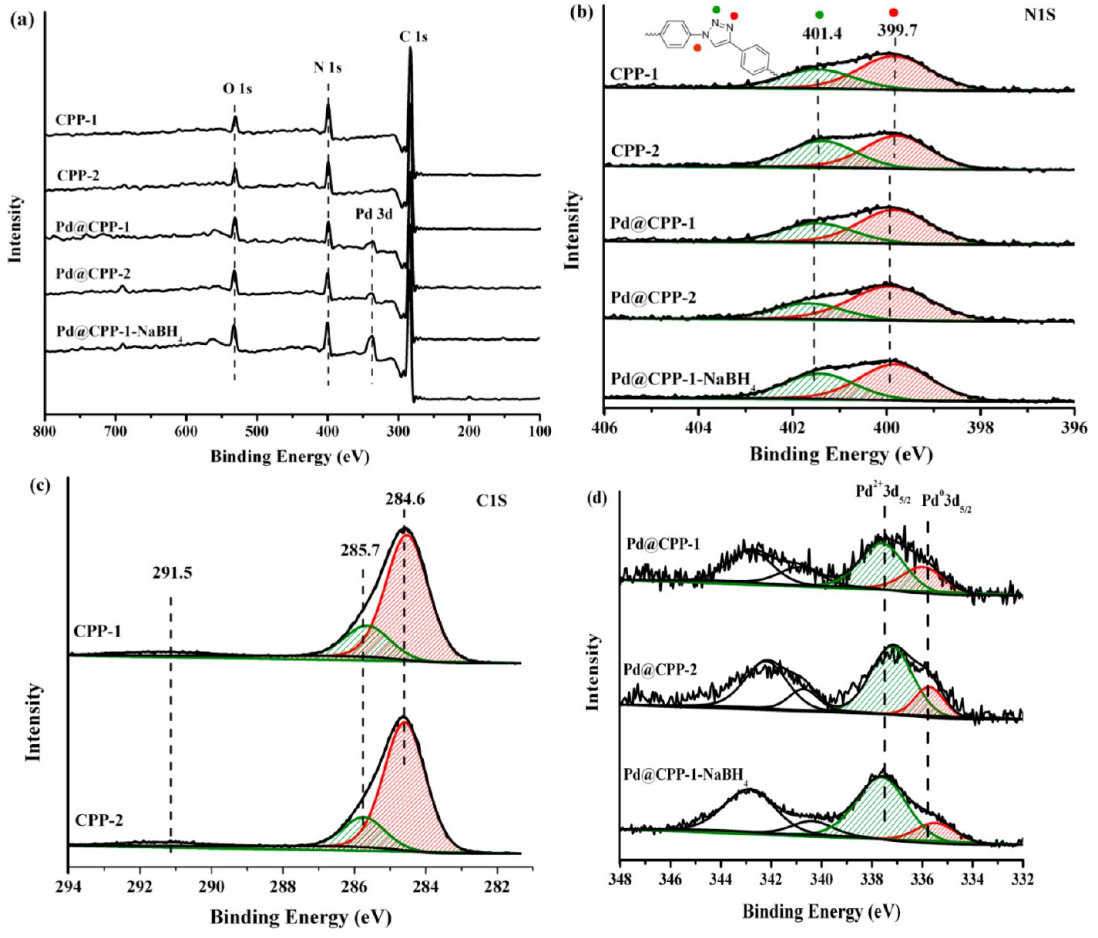

Figure 2. (a) XPS analysis for CPP-1, CPP-2, Pd@CPP-1, Pd@CPP-2, and Pd@CPP-1-$NaBH_4$; (b) N 1s spectra for CPP-1, CPP-2, Pd@CPP-1, Pd@CPP-2, and Pd@CPP-1-$NaBH_4$; (c) C 1s spectra for CPP-1 and CPP-2; (d) Pd 3d spectra for Pd@CPP-1, Pd@CPP-2, and Pd@CPP-1-$NaBH_4$.

respectively (Figure 2a). The N 1s peak can be resolved into two peaks with a ~1:2 intensity ratio, determined by the ratio of their relative peak areas. One peak around 401.4 eV is ascribed to the N2 atom of 1,2,3-triazolyl, and the other peak around 399.7 eV corresponds to N1 and N3 atoms, further suggesting the formation of a 1,2,3-triazolyl ring (Figure 2b).[55,56] This is also well supported by C 1s XPS (Figure 2c); the charge distribution of the carbon atoms is influenced by the neighbor nitrogen atoms. Hence, the C 1s spectra for CPP-1 and CPP-2 could be deconvoluted into two peaks at 284.6 and 285.7 eV, which are assigned to the aromatic carbons and carbon atoms bonded to nitrogen in the triazolyl ring, respectively.[56,57] The peak

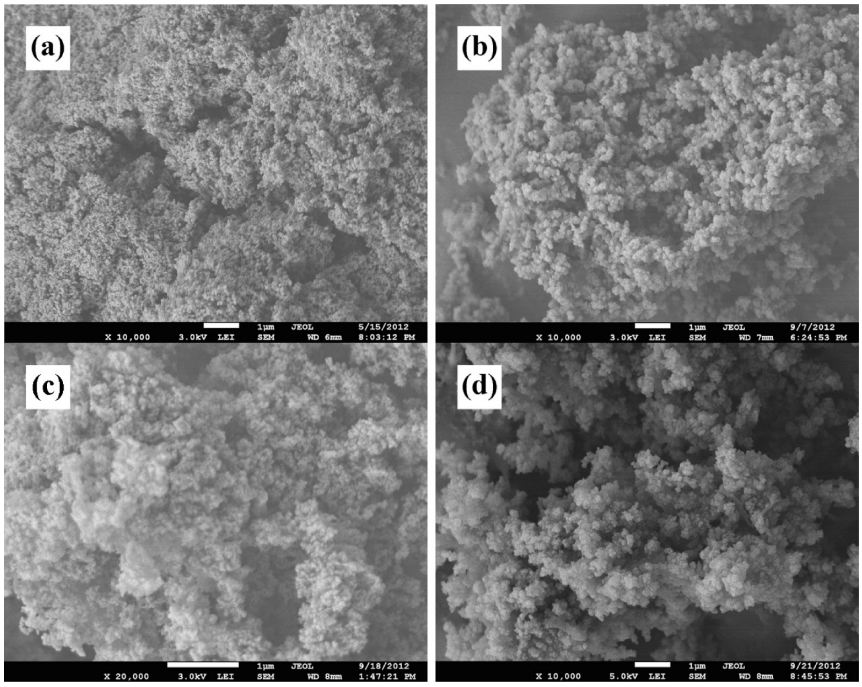

Figure 3. SEM images for (a) CPP-1; (b) CPP-2; (c) Pd@CPP-1; and (d) Pd@CPP-2.

centered at 291.5 eV is attributed to the characteristic shakeup line of the aromatic carbon ($\pi-\pi^*$). The O 1s peak mainly arises from some oxygen or water absorbed onto the surface of the samples.

Scanning electron microscopy (SEM) spectra show that CPP-1 and CPP-2 are composed of granular particles (Figure 3a,b and Figure S3), which is in agreement with most reported POPs constructed by tetrahedral building blocks.[58,59] XRD reveals CPP-1 and CPP-2 are amorphous, ascribed to the kinetically controlled irreversible click reaction process.[49,52]

The porosities of CPP-1 and CPP-2 are determined by N_2 adsorption at 77 K. As shown in Figure S5, a sharp uptake at a relative pressure of $P/P_0 < 0.1$ suggests the presence of extensive microporosity within CPP-1 and CPP-2. The appearance of hysteresis in CPP-1 and CPP-2 isotherms is ascribed to the deformation and swelling of the polymers at 77 K by N_2.[60] The Brunauer–Emmett–Teller (BET) surface areas of CPP-1 and CPP-2 are 826 and 894 $m^2\ g^{-1}$, respectively. The contribution of microporosity to the networks can be calculated as the ratio of micropore volume ($V_{0.1}$) over the total pore volume (V_{tot}).[61] The $V_{0.1}/V_{tot}$ values of CPP-1 and CPP-2 are 0.30 and 0.63, respectively, demonstrating that micropores are more predominant in CPP-2 than in CPP-1 (Table S1), which is in agreement with the shape of N_2 isotherms.

Considering the coordination ability of 1,2,3-triazolyl moieties to metal salts as well as the permanent porosity of the polymers, the immobilization performances of palladium NPs inside the pores of CPP-1 and CPP-2 were investigated (Scheme 1). The treatment of CPP-1 and CPP-2 with $Pd(OAc)_2$ gave rise to brown Pd(II)@CPP-1 and Pd(II)@CPP-2, respectively, and subsequent reduction in a stream of H_2/N_2 afforded gray Pd@CPP-1 and Pd@CPP-2, respectively. Inductively coupled plasma spectroscopy (ICP) analyses show Pd contents in Pd@CPP-1 and Pd@CPP-2 are 0.41 and 0.39 mmol g^{-1}, respectively. Transmission electron microscope (TEM) images show (Figure 4a–f) palladium NPs in Pd@CPP-1 and Pd@CPP-2 are uniformly distributed, and their average sizes are 1.45 ± 0.36 and 1.43 ± 0.34 nm, respectively, which are small enough to be accommodated in the interior cavities of CPP-1 and CPP-2 (Figure S5). HAADF-STEM clearly demonstrates the uniform distribution of ultrafine palladium NPs throughout the interior cavities without deposition on the external surfaces of CPP-1 and CPP-2. Energy-dispersive X-ray (EDX) mapping images reveal that the distribution of palladium NPs is related to the location of N elements, suggesting a high dispersion of palladium NPs in the polymer. As a comparison, palladium NPs immobilized in CPP-1 are also prepared by reduction with $NaBH_4$ (designated as Pd@CPP-1-$NaBH_4$). TEM images exhibit a dual size distribution of palladium NPs. The relatively small palladium NPs, with an average diameter of 1.45 nm, are encapsulated within the pores of CPP-1, while large NPs, with an average diameter of 3.19 nm, are deposited on the external surface of CPP-1 (Figure 4g and h). The dual distribution of Pd@CPP-1-$NaBH_4$ is ascribed to the assumption that the aqueous solution of $NaBH_4$ cannot be drawn efficiently into the pores by capillary force because of the hydrophobic nature of aromatic polymers, and some palladium precursors would be redissolved and diffuse out of the pores, resulting in the formation of large NPs

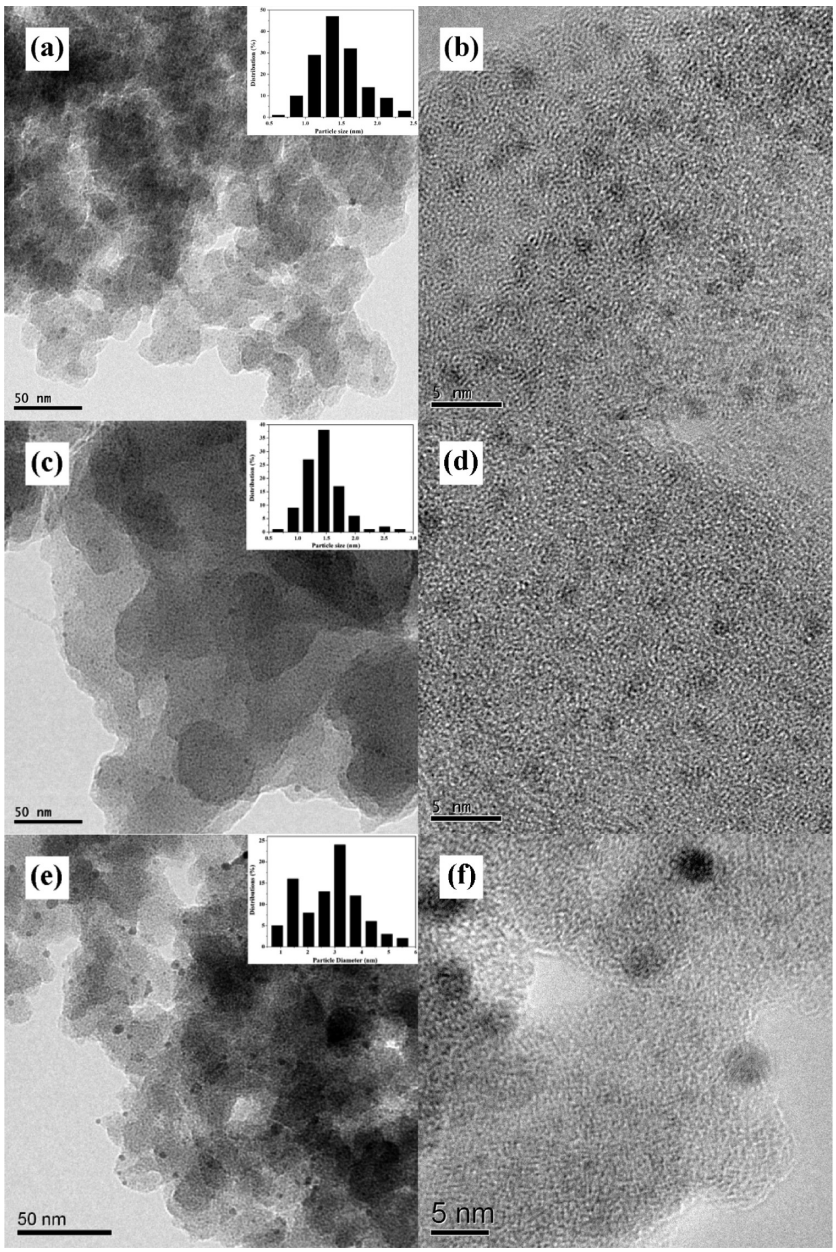

Figure 4. TEM images for (a, b) Pd@CPP-1; (c, d) Pd@CPP-2; and (e, f) Pd@CPP-1-$NaBH_4$.

on the external surface of CPP-1. In contrast, when H_2 is chosen, the particle nucleation can take place within the pores under solid-phase conditions, while, the growth of palladium NPs is confined by the polymers, affording highly dispersed ultrafine palladium NPs without deposition of NPs at the external surface (Scheme 2). Clearly, the preparation method significantly affects the size and dispersion of NPs, and the H_2 reduction method gives the best results in terms of controlling the dispersion and size of NPs in polymers. XRD patterns of Pd@CPP-1, Pd@CPP-2, and Pd@CPP-1-$NaBH_4$ do not exhibit distinct peaks for palladium NPs, revealing the particles are small and well dispersed in the polymers (Figure S4).

In the solid-state ^{13}C NMR spectra of Pd(II)@CPP-1 and Pd(II)@CPP-2 (Figure 1), two new weak signals at 179 and 23 ppm were observed, which are attributed to the carbonyl and methyl carbons of the incorporated $Pd(OAc)_2$, respectively. In comparison with the carbonyl peak of free $Pd(OAc)_2$ at 190 ppm,[34] the chemical shift of carbonyl group of incorporated $Pd(OAc)_2$ is shifted toward high field by 11 ppm, suggesting strong coordination of 1,2,3-triazolyl units to palladium. The characteristic peaks of $Pd(OAc)_2$ in Pd@CPP-1 and Pd@CPP-2 were not observed. Other signals at 110−140 and 64 ppm in Pd(II)@CPP-1, Pd(II)@CPP-2, Pd@CPP-1, and Pd@CPP-2 are assigned to aromatic carbons and the central carbon of the tetraphenylmethane, respectively; they are close to those in CPP-1 and CPP-2, confirming the structural integrity of the polymers. Noteworthy, in comparison with CPP-1

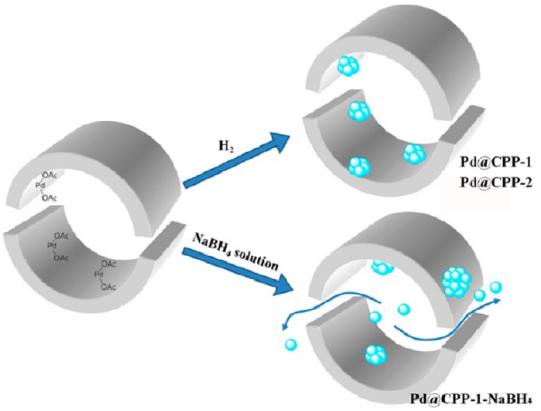

Scheme 2. Schematic representation for immobilization of palladium NPs by CPP-1 and CPP-2.

and CPP-2, the peak envelopes in Pd@CPP-1 and Pd@CPP-2 broaden owing to the interactions between palladium NPs with the aromatic groups.[62] The spectrum for Pd@CPP-2 is very broad relative to CPP-2, which may be ascribed to the significant influence on the electronic properties of polymers by palladium NPs. BET surface areas of Pd@CPP-1 and Pd@CPP-2 are reduced to 444 and 323 $m^2\ g^{-1}$, respectively, and their $V_{0.1}/V_{tot}$ values are simultaneously lowered to 0.20 and 0.52, respectively (Figure S5 and Table S1). The considerable decrements in BET surface area and pore volume demonstrate the successful immobilization of palladium NPs in the interior cavities of the polymers.[34,63,64] Changes in surface area and pore volume between CPP-2 and Pd@CPP-2 are larger than that between CPP-1 and Pd@CPP-1. It seems that the pores in CPP-2 accommodate palladium NPs better than that in CPP-1. The preservation of N_2 adsorption/desorption isotherm shapes indicates that the pore systems have not been blocked or altered substantially by palladium NPs. Signals in IR spectra of Pd@CPP-1 and Pd@CPP-2 are almost identical with those of CPP-1 and CPP-2, indicating that their structures are intact after palladium loading (Figure S1). SEM images show that the original morphologies of CPP-1 and CPP-2 are intact after the incorporation of palladium NPs (Figure 3c and d).

To further illustrate the interactions between 1,2,3-triazolyl units and palladium, XPS was performed. As shown in Figure 2d, Pd 3d spectra present two sets of doublet peaks corresponding to Pd $3d_{5/2}$ and Pd $3d_{3/2}$. The Pd $3d_{5/2}$ peaks at 335.97 and 335.72 eV in Pd@CPP-1 and Pd@CPP-2 are attributed to Pd^0 species, respectively, while the Pd $3d_{5/2}$ peaks at 337.58 and 337.20 eV are related to their Pd^{2+} species. The ratios of Pd^0/Pd^{2+} in Pd@CPP-1 and Pd@CPP-2 are 0.56 and 0.31, respectively. In comparison with CPP-1 and CPP-2, the N 1s peak in Pd@CPP-1 and Pd@CPP-2 shifts from 399.78 to 399.83 eV and from 399.77 to 399.91 eV, respectively (Figure 2b). The upshift of the N 1s toward higher binding energies is attributed to the coordination of nitrogen atoms to palladium.[65] It seems that the interaction between palladium NPs and nitrogen atoms in Pd@CPP-2 is stronger than that in Pd@CPP-1, which is consistent with the aforementioned more broaden peaks of Pd@CPP-2 than Pd@CPP-1 in the solid-state ^{13}C NMR spectra.

To further investigate the effect of substituent variation at 1,2,3-triazolyl ring on the electronic characters of polymers and the interactions between polymers and palladium NPs, natural bond orbital (NBO) analyses based on the optimized structures of their model compounds (CPP-1-MC, CPP-2-MC, Pd@CPP-1-MC, and Pd@CPP-2-MC) were performed with Gaussian 03 (Figure S7). As shown in Figure 5 and Table S2, all nitrogen atoms in model compounds carry a negative charge. The N3 atom possesses the most negative charge in the triazolyl ring and should preferably coordinate to palladium. The triazolyl group carries a negative charge, while phenyl and tetraphenylmethane groups have positive charges. The charges of the 1,2,3-triazolyl group and N3 atom in CPP-2-MC are both slightly more negative than those in CPP-1-MC, which may lead to stronger coordination abilities to palladium. As expected, palladium in Pd@CPP-2-MC carries more negative charges than that in Pd@CPP-1-MC. Notably, palladium in Pd@CPP-1-MC is stericly crowded by a tetraphenylmethane group, while palladium in Pd@CPP-2-MC is relatively less steric. Substituents at the N1 position of the 1,2,3-triazolyl ring in CPP-1-MC and CPP-2-MC have more positive charges than substituents at the C4 position due to the inductive electron-withdrawing effect of the N1 atom. In comparison with analogues in CPP-1-MC and CPP-2-MC, substituents at the N1 position of the 1,2,3-triazolyl ring in Pd@CPP-1-MC and Pd@CPP-2-MC have more positive charges, while substituents at the C4 position of the 1,2,3-triazolyl ring have more negative charges. The charge of the tetraphenylmethane group in Pd@CPP-1-MC is less positive than that in Pd@CPP-2-MC, while the charge of the phenyl group in Pd@CPP-1-MC is more positive than that in Pd@CPP-2-MC. These differences of charge distribution in model compounds suggest different electron properties of CPP-1, CPP-2, Pd@CPP-1, and Pd@CPP-2. The results of charge distributions are consistent with the broadened peaks in the solid-state ^{13}C NMR of Pd@CPP-1 and Pd@CPP-2 and the results of their XPS analyses. These results show that variation of the tetraphenylmethane group at the 1,2,3-triazolyl ring has a significant influence on the steric and electronic properties of polymers and the interactions between polymers and palladium NPs. Considering the combination of more negative charges and less steric hindrance, palladium atoms in Pd@CPP-2 may be more reactive in catalytic reactions than Pd@CPP-1.

The HOMO and LUMO analyses reveal that the HOMO and LUMO are shared by triazolyl and its phenyl groups in CPP-1-MC and CPP-2-MC owing to their conjugative effects. Interestingly, HOMOs in

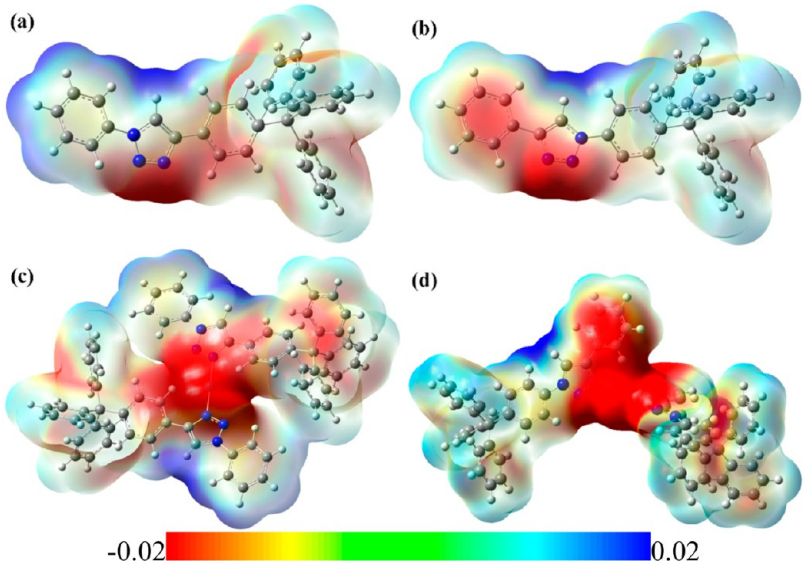

Figure 5. Charge distributions in CPP-1-MC (a), CPP-2-MC (b), Pd@CPP-1-MC (c), and Pd@CPP-2-MC (d). The numbers represent energy per charge in units of hartree per elemental charge.

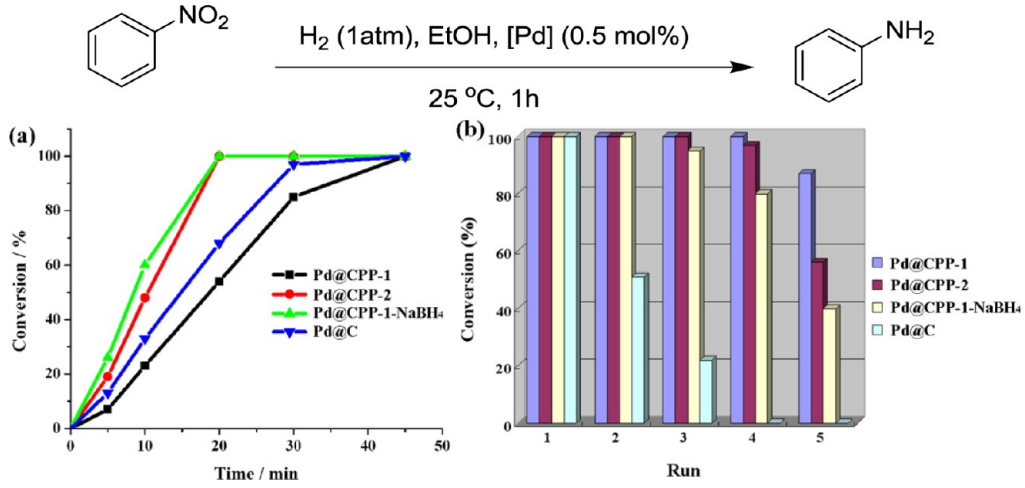

Figure 6. (a) Conversion of nitrobenzene as a function of time in hydrogenation reactions. (b) Reusability of Pd@CPP-1, Pd@CPP-2, Pd@CPP-1-$NaBH_4$, and Pd@C. Reaction conditions: nitrobenzene (0.5 mmol), [Pd] (0.5 mol %), ethanol (2 mL), 1 atm of H_2, 25 °C, 1 h.

Pd@CPP-1-MC and Pd@CPP-2-MC are mainly occupied by a palladium atom, and LUMOs are shared by triazolyl and its N-substituted phenyl ring (Figure S8).

It is well known that the size and location of supported palladium NPs have an important effect on their catalytic activity. The catalytic performances of Pd@CPP-1, Pd@CPP-2, and Pd@CPP-1-$NaBH_4$ were investigated by hydrogenation of nitroarenes at 25 °C under 1 atm. As shown in Figure 5a, Pd@CPP-1 afforded full conversion of nitrobenzene to aniline within 45 min, while the use of Pd@CPP-2 under the same conditions gave rise to a complete conversion within 20 min. The higher activity of Pd@CPP-2 than Pd@CPP-1 probably results from the synergistic effects of relatively more negative charges and less steric hindrance of palladium NPs. Interestingly, when Pd@CPP-1-$NaBH_4$ was employed, a quantitative conversion was achieved within 20 min, which is similar to Pd@CPP-2. A possible reason for this observation is that nitrobenzene can directly access palladium NPs deposited on the external surface of Pd@CPP-1-$NaBH_4$. For comparison, commercial palladium on charcoal (Pd@C) was also tested under the same conditions, and a complete conversion of nitrobenzene within 45 min was achieved. Besides catalytic activity, recyclability is also crucial for an outstanding heterogeneous catalysis. As shown in Figure 5b, Pd@CPP-1 could be reused at least five times. However, the conversion of nitrobenzene in Pd@CPP-2 and Pd@CPP-1-$NaBH_4$ was decreased to 97% and 95% after the fourth run and the third run, respectively. When Pd@C was used, the conversion of nitrobenzene decreased to 50% and 20% in the second and third runs, respectively.

TEM images show that palladium NPs after the fifth run reaction in Pd@CPP-1 and Pd@CPP-2 are all

TABLE 1. Reduction of Various Nitroarenes[a,b,c,d,e,f,g]

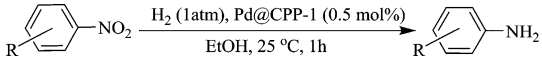

Entry	Reactant	Product	Conv. (%)[b]	Select. (%)
1	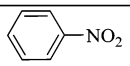	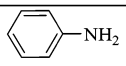	100(98)	100
2[c]	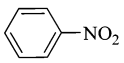	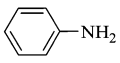	0	0
3	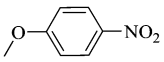	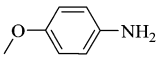	100(100)	100
4	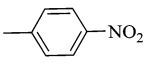	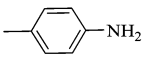	100(90)	100
5	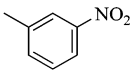	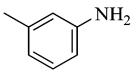	100(95)	100
6	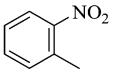	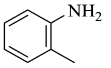	85-	85
7	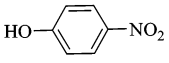	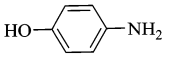	100(95)	100
8[d]	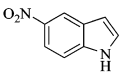	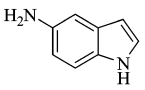	-(85)	-
9[d]	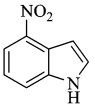	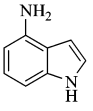	-(61)	-
10	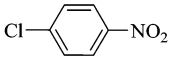	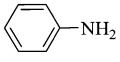	66-	100
11[e]	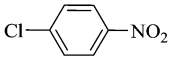	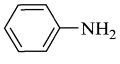	100-	100
12[f]	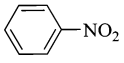	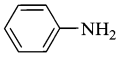	18-	-
13[g]	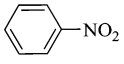	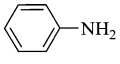	19-	-

[a] Reaction conditions: nitroarenes (0.5 mmol), Pd@CPP-1 (0.5 mol %), ethanol (2 mL), 1 atm of H_2, 25 °C, 1 h. [b] GC yield; isolated yields are given in parentheses. [c] Without palladium. [d] 5 h. [e] 3 h. [f] 5 min. [g] After 5 min, the reaction of filtration was performed for an additional 15 h.

well-dispersed (Figure 6a−d). Their average sizes are 1.71 ± 0.46 nm and 1.90 ± 0.56 nm, respectively, which are only slightly larger than that in fresh Pd@CPP-1 and Pd@CPP-2 (Figure 4). However, for Pd@CPP-1-$NaBH_4$, after the fifth run, the average diameters of palladium NPs on the surface of the support increased from 3.19 nm to 5.03 nm (Figure 6e and f). It further reveals that the stabilization of palladium NPs is ascribed to the synergistic effects of the coordination of 1,2,3-triazolyl and the nanoscale confinement effect of polymers.

To explore the generality of the catalytic system, nitroarenes bearing different steric and electronic characters were tested. As shown in Table 1, when the reaction was carried out in the presence of 0.5 mol % Pd@CPP-1 at 25 °C, 98% isolated yield of aniline was obtained in 1 h (entry 1). No aniline was formed in the

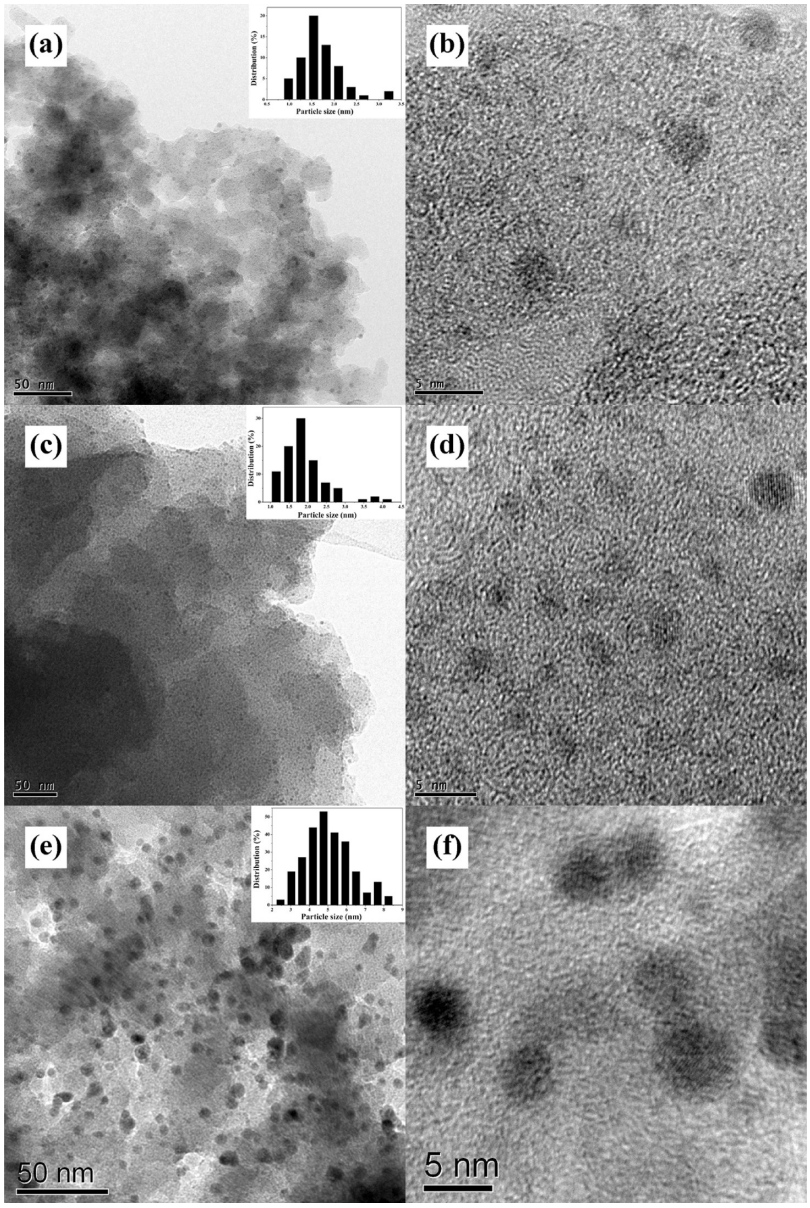

Figure 7. TEM images for (a, b) Pd@CPP-1 after the fifth run; (c, d) Pd@CPP-2 after the fifth run; and (e, f) Pd@CPP-1-$NaBH_4$ after the fifth run.

control experiment of nitrobenzene in the absence of Pd@CPP-1 (entry 2). 4-Nitroanisole, 4-nitrotoluene, and 3-nitrotoluene were reduced into corresponding products in full conversion and selectivity (entries 3−5), while reduction of 2-nitrotoluene gave rise to 2-methylaniline in 85% GC (gas chromatography) yield (entry 6) owing to the steric effect. Interestingly, a hydroxyl group can be well tolerated in the catalytic system (entry 7). The catalytic system is also effective for reduction of heterocyclic nitro compounds. When 4-nitroindole and 5-nitroindole were used as substrates, the corresponding products were obtained in 85% and 61% isolated yields, respectively (entries 8 and 9). The reduction of 4-nitrochlorobenzene gave rise to the dechloro product aniline in a 66% yield in 1 h, and 100% yield was obtained in 3 h (entries 10 and 11). This tendency toward dehalogenation was often observed in palladium-catalyzed hydrogenation of aryl halides.[12,66]

To ensure that the immobilized palladium NPs represent the catalytically active species rather than free palladium that is dissociated from the polymers during reaction, a hot filtration test was performed. After the reaction was run for 5 min, Pd@CPP-1 was removed from the reaction mixture by filtration, and the filtrate continued to react for an additional 15 h. Negligible changes in conversion and selectivity were observed (entries 13 and 14, Table 1). ICP analysis of the filtrate shows that palladium leaching is 0.48 ppm, which is insignificant with respect to 0.41 mmol g^{-1} of fresh Pd@CPP-1.

CONCLUSION

Two click-based porous organic polymers (CPP-1 and CPP-2) have been readily synthesized. Size- and

location-controllable ultrafine palladium NPs are facilely immobilized inside the pores of CPP-1 and CPP-2. In comparison with palladium NPs with dual distributions and palladium on charcoal, no obvious aggregation and loss of catalytic activity of ultrafine palladium NPs were observed after the catalytic reaction was recycled several times. The synergistic effects of the coordination of 1,2,3-triazolyl to palladium and the confinement effect of polymers result in good stabilization of palladium NPs. The variation of the tetraphenylmethane group at the 1,2,3-triazolyl ring shows important influence on the steric and electronic properties of polymers as well as the interaction between frameworks and palladium NPs, and hence the catalytic performance of palladium NPs. Palladium NPs in Pd@CPP-2 show relatively more negative charges and less steric hindrance than NPs in Pd@CPP-1, resulting in higher catalytic activity. In summary, this study not only provides a general and facile approach for fabrication of ultrafine metal NPs with size- and location-control but also opens a new avenue to development of efficiently heterogeneous catalytic systems by using POPs as supports of metal NPs.

METHODS

General Information. Tetrakis(4-azidophenyl)methane,[49] 4,4′-diazidobiphenyl,[49] tetrakis(4-ethynylphenyl)methane,[67] and 4,4′-diethynylbiphenyl[68] were prepared according to literature methods. Pd@C was purchased from Aladdin Industrial Corporation (Shanghai, China). Other chemicals were commercially available and used without further purification. ^{1}H and ^{13}C NMR spectra were recorded on a Bruker AVANCE III NMR spectrometer at 400 and 100 MHz, respectively, using tetramethylsilane (TMS) as an internal standard. Solid-state ^{13}C CP/MAS NMR was performed on a Bruker SB Avance III 500 MHz spectrometer with a 4 mm double-resonance MAS probe, a sample spinning rate of 7.0 kHz, a contact time of 2 ms, and a pulse delay of 5 s. IR spectra were recorded with KBr pellets using a PerkinElmer instrument. Thermal gravimetric analysis (TGA) was carried out on a NETZSCH STA 449C by heating samples from 30 to 700 °C in a dynamic nitrogen atmosphere with a heating rate of 10 °C min^{-1}. Powered X-ray diffraction (XRD) patterns were recorded in the range of $2\theta = 5-40°$ on a desktop X-ray diffractometer (RIGAKU-Miniflex II) with Cu Kα radiation (λ = 1.5406 Å). Nitrogen adsorption and desorption isotherms were measured at 77 K using a Micromeritics ASAP 2020 system. The samples were degassed at 100 °C for 5 h before the measurements. Surface areas were calculated from the adsorption data using Brunauer–Emmett–Teller. The pore size distribution curves were obtained from the adsorption branches using the nonlocal density functional theory method. Field-emission scanning electron microscopy was performed on a JEOL JSM-7500F operated at an accelerating voltage of 3.0 kV. Transmission electron microscope high-annular dark-field scanning (HAADF-STEM) and energy-dispersive X-ray mapping images were obtained with a TECNAI G^2 F20 equipped with an EDX detector. X-ray photoelectron spectroscopy measurements were performed on a Thermo ESCALAB 250 spectrometer, using nonmonochromatic Al Kα X-rays as the excitation source and choosing C 1s (284.6 eV) as the reference line. Inductively coupled plasma spectroscopy was measured on a Jobin Yvon Ultima2. Gas chromatography was performed on a Shimadzu GC-2014 equipped with a capillary column (RTX-5, 30 m × 0.25 μm) using a flame ionization detector. Elemental analyses were performed on an Elementar Vario MICRO elemental analyzer.

Synthesis of CPP-1. To a solution of tetrakis(4-ethynylphenyl)-methane (0.74 g, 1.8 mmol), 4,4′-diazidobiphenyl (0.84 g, 3.6 mmol), and $CuSO_4 \cdot 5H_2O$ (0.18 g, 0.7 mmol) in DMF (100 mL), was added sodium ascorbate (0.14 g, 0.7 mmol) under a N_2 atmosphere. The stirring mixture was heated to 100 °C and maintained at that temperature for 3 days. The brown precipitate was isolated by filtration, rinsed with DMF (2 × 30 mL) and methanol (2 × 30 mL), and then redispersed in saturated EDTA-2Na solution (20 mL) at room temperature for 12 h. After filtering and washing with excess H_2O and methanol, the resultant material was purified by Soxhlet extraction using THF and dried *in vacuo* at 80 °C for 12 h to afford CPP-1 as a brown powder, 1.4 g, yield 89%. IR (KBr, cm^{-1}): 3143 (w), 3050 (w), 2926 (w), 2129 (w), 2097 (w), 1610 (s), 1490 (vs), 1402 (m), 1227 (s), 1116 (w), 1042 (s), 827 (vs), 736 (vw), 564 (vw). Anal. Calcd (%) for $(C_{14.25}H_9N_3)_n$: C 77.01, H 4.09, N 18.91. Found: C 65.13, H 5.33, N 15.15.

Synthesis of CPP-2. Following the same procedures as for the synthesis of CPP-1, CPP-2 was obtained as a yellow solid. Yield: 100%. IR (KBr, cm^{-1}): 3422 (s), 3144 (w), 2363 (w), 2326 (w), 2123 (m), 1918 (vw), 1608 (s), 1512 (vs), 1482 (s), 1407 (m) 1289 (w), 1227(m), 1117 (w), 1042 (s), 994 (s), 827 (vs), 741 (w), 668 (vw), 532 (w). Anal. Calcd (%) for $(C_{14.25}H_9N_3)_n$: C 77.01, H 4.09, N 18.91. Found: C 72.19, H 4.86, N 17.23.

Synthesis of Pd(II)@CPP-1 and Pd@CPP-1. To a solution of $Pd(OAc)_2$ (81 mg, 0.36 mmol) in dichloromethane (100 mL) was added CPP-1 (200 mg). After stirring at 60 °C for 24 h, the precipitate was isolated by filtration, purified by Soxhlet extraction using dichloromethane, and dried *in vacuo* at 80 °C for 12 h to give Pd(II)@CPP-1 as a brown solid. Pd(II)@CPP-1 was reduced in a stream of H_2/N_2 (10% H_2, 100 mL/min^{-1}) at 200 °C for 4 h to give Pd@CPP-1 as a gray solid. The Pd content in Pd@FCP-1 was 0.41 mmol g^{-1} as determined by ICP.

Synthesis of Pd(II)@CPP-2 and Pd@CPP-2. Following the same procedures as for the synthesis of Pd(II)@CPP-1 and Pd@CPP-1, Pd(II)@CPP-2 and Pd@CPP-2 were obtained as a brown solid and gray solid, respectively. The Pd content in Pd@FCP-1 was 0.39 mmol g^{-1} as determined by ICP.

Synthesis of Pd@CPP-1-$NaBH_4$. To a solution of $Pd(OAc)_2$ (81 mg, 0.36 mmol) in dichloromethane (100 mL) was added CPP-1 (200 mg). After stirring at 60 °C for 24 h, the precipitate was isolated by filtration, purified by Soxhlet extraction with dichloromethane, and dried *in vacuo* at 80 °C for 12 h. To a vigorous stirring dispersion of the reultant brown solid (100 mg) in water (100 mL), a freshly prepared 1 M aqueous $NaBH_4$ solution (1 mL) was added. The suspension was collected by centrifugation and dried at 80 °C *in vacuo* to give Pd@CPP-1-$NaBH_4$ as a gray solid. The Pd content in Pd@CPP-1-$NaBH_4$ was 0.53 mmol g^{-1} as determined by ICP.

Typical Procedure for Hydrogenation of Nitroarenes. Nitroarene (0.5 mmol), Pd-containing samples (0.5 mol %), and ethanol (2.0 mL) were placed in a Schlenk flask (20 mL). The flask was purged with H_2 three times to remove air, and the reaction mixture was stirred with a balloon of H_2 at room temperature for a given time. After the reaction, the resultant mixture was transferred into a tube and the solid was separated by centrifugation. The organic phase was analyzed with GC to determine conversion and selectivity. The identity of products was confirmed by comparison with GC retention times of commercial materials and literature NMR spectroscopic data.

Recyclability Tests for Hydrogenation of Nitrobenzene. After the first run reaction was finished, the residual solid was recovered by centrifugation and washed with ethanol, followed by centrifugation. The processes were repeated twice, and the resultant solid was directly used for the next run with the same amount of fresh nitrobenzene and ethanol.

Theoretical Calculations. The density functional theory (DFT) method at the hybrid Becke three-parameter Lee–Yang–Parr (B3LYP) functional level was used to study the electronic

structures of model compounds (CPP-1-MC, CPP-2-MC, Pd@CPP-1-MC, and Pd@CPP-2-MC). The geometrical structures were first optimized. During the calculation processes, the symmetry restrictions of the structures were not considered, and the convergent values of maximum force, root-mean-square (RMS) force, maximum displacement, and RMS displacement were set by default. Then, the natural bond orbital analysis was implemented. In these calculations, the Lanl2dz effective core potential was used to describe the inner electrons of palladium atoms, while its associated double-ζ basis set of Hay and Wadt was employed for the remaining outer electrons. The all-electron basis set of 6-31G* was used for nonmetal N, C, and H atoms. All calculations were implemented in the Gaussian 03 program.[69] Visualization of the optimized geometrical structures, frontier molecular orbitals, and electrostatic potential mapped onto the electron density surface were performed by GaussView.

Conflict of Interest: The authors declare no competing financial interest.

Supporting Information Available: Gas adsorption isotherms, structure characterizations, EDX and TEM images, and theoretical calculations of model compounds. This material is available free of charge *via* the Internet at http://pubs.acs.org.

Acknowledgment. The authors acknowledge the 973 Program (2011CBA00502, 2010CB933501), National Natural Science Foundation of China (21273239), Natural Science Foundation of Fujian Province (2011J01064), and "One Hundred Talent Project" from the Chinese Academy of Sciences for financial support.

REFERENCES AND NOTES

1. Zaera, F. Nanostructured Materials for Applications in Heterogeneous Catalysis. *Chem. Soc. Rev.* **2013**, *42*, 2746–2762.
2. Dhakshinamoorthy, A.; Garcia, H. Catalysis by Metal Nanoparticles Embedded on Metal-Organic Frameworks. *Chem. Soc. Rev.* **2012**, *41*, 5262–5284.
3. Burda, C.; Chen, X.; Narayanan, R.; El-Sayed, M. A. Chemistry and Properties of Nanocrystals of Different Shapes. *Chem. Rev.* **2005**, *105*, 1025–1102.
4. Vajda, S.; Pellin, M. J.; Greeley, J. P.; Marshall, C. L.; Curtiss, L. A.; Ballentine, G. A.; Elam, J. W.; Catillon-Mucherie, S.; Redfern, P. C.; Mehmood, F. Subnanometre Platinum Clusters as Highly Active and Selective Catalysts for the Oxidative Dehydrogenation of Propane. *Nat. Mater.* **2009**, *8*, 213–216.
5. Qiao, B.; Wang, A.; Yang, X.; Allard, L. F.; Jiang, Z.; Cui, Y.; Liu, J.; Li, J.; Zhang, T. Single-Atom Catalysis of CO Oxidation Using Pt1/FeOx. *Nat. Chem.* **2011**, *3*, 634–641.
6. Li, Z.; Liu, J.; Xia, C.; Li, F. Nitrogen-Functionalized Ordered Mesoporous Carbons as Multifunctional Supports of Ultrasmall Pd Nanoparticles for Hydrogenation of Phenol. *ACS Catal.* **2013**, 2440–2448.
7. Kibata, T.; Mitsudome, T.; Mizugaki, T.; Jitsukawa, K.; Kaneda, K. Investigation of Size-Dependent Properties of Sub-Nanometer Palladium Clusters Encapsulated within a Polyamine Dendrimer. *Chem. Commun.* **2013**, *49*, 167–169.
8. White, R. J.; Luque, R.; Budarin, V. L.; Clark, J. H.; Macquarrie, D. J. Supported Metal Nanoparticles on Porous Materials. Methods and Applications. *Chem. Soc. Rev.* **2009**, *38*, 481–494.
9. Ott, L. S.; Finke, R. G. Transition-Metal Nanocluster Stabilization for Catalysis: A Critical Review of Ranking Methods and Putative Stabilizers. *Coord. Chem. Rev.* **2007**, *251*, 1075–1100.
10. Pileni, M.-P. The Role of Soft Colloidal Templates in Controlling the Size and Shape of Inorganic Nanocrystals. *Nat. Mater.* **2003**, *2*, 145–150.
11. Gascon, J.; Aktay, U.; Hernandezalonso, M.; Vanklink, G.; Kapteijn, F. Amino-Based Metal-Organic Frameworks as Stable, Highly Active Basic Catalysts. *J. Catal.* **2009**, *261*, 75–87.
12. Cárdenas-Lizana, F.; Berguerand, C.; Yuranov, I.; Kiwi-Minsker, L. Chemoselective Hydrogenation of Nitroarenes: Boosting Nanoparticle Efficiency by Confinement within Highly Porous Polymeric Framework. *J. Catal.* **2013**, *301*, 103–111.
13. Li, X.-H.; Antonietti, M. Metal Nanoparticles at Mesoporous N-Doped Carbons and Carbon Nitrides: Functional Mott-Schottky Heterojunctions for Catalysis. *Chem. Soc. Rev.* **2013**, *42*, 6593–6604.
14. Liu, B.; Jie, S. Y.; Li, B. G. Metal-Organic Frameworks for Heterogeneous Catalysis. *Prog. Chem.* **2013**, *25*, 36–45.
15. Vilhelmsen, L. B.; Walton, K. S.; Sholl, D. S. Structure and Mobility of Metal Clusters in MOFs: Au, Pd, and AuPd Clusters In MOF-74. *J. Am. Chem. Soc.* **2012**, *134*, 12807–12816.
16. Aijaz, A.; Karkamkar, A.; Choi, Y. J.; Tsumori, N.; Ronnebro, E.; Autrey, T.; Shioyama, H.; Xu, Q. Immobilizing Highly Catalytically Active Pt Nanoparticles inside the Pores of Metal-Organic Framework: A Double Solvents Approach. *J. Am. Chem. Soc.* **2012**, *134*, 13926–13929.
17. Zhu, Q. L.; Li, J.; Xu, Q. Immobilizing Metal Nanoparticles to Metal-Organic Frameworks with Size and Location Control for Optimizing Catalytic Performance. *J. Am. Chem. Soc.* **2013**, *135*, 10210–10213.
18. Lu, G.; Li, S.; Guo, Z.; Farha, O. K.; Hauser, B. G.; Qi, X.; Wang, Y.; Wang, X.; Han, S.; Liu, X. Imparting Functionality to a Metal-Organic Framework Material by Controlled Nanoparticle Encapsulation. *Nat. Chem.* **2012**, *4*, 310–316.
19. Moon, H. R.; Lim, D. W.; Suh, M. P. Fabrication of Metal Nanoparticles in Metal-Organic Frameworks. *Chem. Soc. Rev.* **2013**, *42*, 1807–1824.
20. Ma, L.; Lin, W. Designing Metal-Organic Frameworks for Catalytic Applications. *Top. Curr. Chem.* **2010**, *293*, 175–205.
21. Peterson, G. W.; Wagner, G. W.; Balboa, A.; Mahle, J.; Sewell, T.; Karwacki, C. J. Ammonia Vapor Removal by $Cu_3(BTC)_2$ and Its Characterization by MAS NMR. *J. Phys. Chem. C* **2009**, *113*, 13906–13917.
22. Zou, X. Q.; Ren, H.; Zhu, G. S. Topology-Directed Design of Porous Organic Frameworks and their Advanced Applications. *Chem. Commun.* **2013**, *49*, 3925–3936.
23. Dawson, R.; Cooper, A. I.; Adams, D. J. Nanoporous Organic Polymer Networks. *Prog. Polym. Sci.* **2012**, *37*, 530–563.
24. Patel, H. A.; Karadas, F.; Byun, J.; Park, J.; Deniz, E.; Canlier, A.; Jung, Y.; Atilhan, M.; Yavuz, C. T. Highly Stable Nanoporous Sulfur-Bridged Covalent Organic Polymers for Carbon Dioxide Removal. *Adv. Funct. Mater.* **2013**, *23*, 2270–2276.
25. Zhao, H.; Jin, Z.; Su, H.; Zhang, J.; Yao, X.; Zhao, H.; Zhu, G. Target Synthesis of a Novel Porous Aromatic Framework and Its Highly Selective Separation of CO(2)/CH(4). *Chem. Commun.* **2013**, *49*, 2780–2782.
26. Fang, Q.; Gu, S.; Zheng, J.; Zhuang, Z.; Qiu, S.; Yan, Y. 3D Microporous Base-Functionalized Covalent Organic Frameworks for Size-Selective Catalysis. *Angew. Chem., Int. Ed.* **2014**, *53*, 2878–2882.
27. Jiang, J. X.; Wang, C.; Laybourn, A.; Hasell, T.; Clowes, R.; Khimyak, Y. Z.; Xiao, J.; Higgins, S. J.; Adams, D. J.; Cooper, A. I. Metal-Organic Conjugated Microporous Polymers. *Angew. Chem., Int. Ed.* **2011**, *50*, 1072–1075.
28. Chen, L.; Yang, Y.; Jiang, D. CMPs as Scaffolds for Constructing Porous Catalytic Frameworks: a Built-in Heterogeneous Catalyst with High Activity and Selectivity Based on Nanoporous Metalloporphyrin Polymers. *J. Am. Chem. Soc.* **2010**, *132*, 9138–9143.
29. Ding, S. Y.; Wang, W. Covalent Organic Frameworks (COFs): From Design to Applications. *Chem. Soc. Rev.* **2013**, *42*, 548–568.
30. Medina, D. D.; Werner, V.; Auras, F.; Tautz, R.; Dogru, M.; Schuster, J.; Linke, S.; Doblinger, M.; Feldmann, J.; Knochel, P.; *et al.* Oriented Thin Films of a Benzodithiophene Covalent Organic Framework. *ACS Nano* **2014**, 10.1021/nn5000223.
31. Zhang, Y. G.; Riduan, S. N. Functional Porous Organic Polymers for Heterogeneous Catalysis. *Chem. Soc. Rev.* **2012**, *41*, 2083–2094.

32. Li, Z.; Liu, J.; Huang, Z.; Yang, Y.; Xia, C.; Li, F. One-Pot Synthesis of Pd Nanoparticle Catalysts Supported on N-Doped Carbon and Application in the Domino Carbonylation. *ACS Catal.* **2013**, *3*, 839–845.
33. Zhang, P.; Weng, Z.; Guo, J.; Wang, C. Solution-Dispersible, Colloidal, Conjugated Porous Polymer Networks with Entrapped Palladium Nanocrystals for Heterogeneous Catalysis of the Suzuki-Miyaura Coupling Reaction. *Chem. Mater.* **2011**, *23*, 5243–5249.
34. Ding, S. Y.; Gao, J.; Wang, Q.; Zhang, Y.; Song, W. G.; Su, C. Y.; Wang, W. Construction of Covalent Organic Framework for Catalysis: Pd/COF-LZU1 in Suzuki-Miyaura Coupling Reaction. *J. Am. Chem. Soc.* **2011**, *133*, 19816–19822.
35. Hasell, T.; Wood, C. D.; Clowes, R.; Jones, J. T. A.; Khimyak, Y. Z.; Adams, D. J.; Cooper, A. I. Palladium Nanoparticle Incorporation in Conjugated Microporous Polymers by Supercritical Fluid Processing. *Chem. Mater.* **2010**, *22*, 557–564.
36. Zhang, Q.; Yang, Y.; Zhang, S. Novel Functionalized Microporous Organic Networks Based on Triphenylphosphine. *Chem.—Eur. J.* **2013**, *19*, 10024–10029.
37. Chan-Thaw, C. E.; Villa, A.; Prati, L.; Thomas, A. Triazine-Based Polymers as Nanostructured Supports for the Liquid-Phase Oxidation of Alcohols. *Chem.—Eur. J.* **2011**, *17*, 1052–1057.
38. Zhou, Y.; Xiang, Z.; Cao, D.; Liu, C. J. Covalent Organic Polymer Supported Palladium Catalysts for CO Oxidation. *Chem. Commun.* **2013**, *49*, 5633–5635.
39. Chan-Thaw, C. E.; Villa, A.; Katekomol, P.; Su, D.; Thomas, A.; Prati, L. Covalent Triazine Framework as Catalytic Support for Liquid Phase Reaction. *Nano Lett.* **2010**, *10*, 537–541.
40. Xie, Z.; Wang, C.; deKrafft, K. E.; Lin, W. Highly Stable and Porous Cross-Linked Polymers for Efficient Photocatalysis. *J. Am. Chem. Soc.* **2011**, *133*, 2056–2059.
41. Wan, Y.; Wang, H.; Zhao, Q.; Klingstedt, M.; Terasaki, O.; Zhao, D. Ordered Mesoporous Pd/Silica-Carbon as a Highly Active Heterogeneous Catalyst for Coupling Reaction of Chlorobenzene in Aqueous Media. *J. Am. Chem. Soc.* **2009**, *131*, 4541–4550.
42. Liang, L.; Astruc, D. The Copper(I)-Catalyzed Alkyne-Azide Cycloaddition (CuAAC) "Click" Reaction and Its Applications. An Overview. *Coord. Chem. Rev.* **2011**, *255*, 2933–2945.
43. Barner-Kowollik, C.; Du Prez, F. E.; Espeel, P.; Hawker, C. J.; Junkers, T.; Schlaad, H.; Van Camp, W. "Clicking" Polymers or Just Efficient Linking: What is the Difference? *Angew. Chem., Int. Ed.* **2011**, *50*, 60–62.
44. Juríček, M.; Kouwer, P. H. J.; Rowan, A. E. Triazole: A Unique Building Block for the Construction of Functional Materials. *Chem. Commun.* **2011**, *47*, 8740–8749.
45. Juríček, M.; Felici, M.; Contreras-Carballada, P.; Lauko, J.; Bou, S. R.; Kouwer, P. H. J.; Brouwer, A. M.; Rowan, A. E. Triazole-Pyridine Ligands: A Novel Approach to Chromophoric Iridium Arrays. *J. Mater. Chem.* **2011**, *21*, 2104–2111.
46. Fleischel, O.; Wu, N.; Petitjean, A. Click-Triazole: Coordination of 2-(1,2,3-Triazol-4-yl)-Pyridine to Cations of Traditional Tetrahedral Geometry (Cu(I), Ag(I)). *Chem. Commun.* **2010**, *46*, 8454–8456.
47. Wang, D.; Denux, D.; Ruiz, J.; Astruc, D. The Clicked Pyridyl-Triazole Ligand: From Homogeneous to Robust, Recyclable Heterogeneous Mono- and Polymetallic Palladium Catalysts for Efficient Suzuki-Miyaura, Sonogashira, and Heck Reactions. *Adv. Synth. Catal.* **2013**, *355*, 129–142.
48. Li, L. Y.; Wang, J. Y.; Wu, T.; Wang, R. H. Click Ionic Liquids: A Family of Promising Tunable Solvents and Application in Suzuki-Miyaura Cross-Coupling. *Chem.—Eur. J.* **2012**, *18*, 7842–7851.
49. Pandey, P.; Farha, O. K.; Spokoyny, A. M.; Mirkin, C. A.; Kanatzidis, M. G.; Hupp, J. T.; Nguyen, S. T. A "Click-Based" Porous Organic Polymer from Tetrahedral Building Blocks. *J. Mater. Chem.* **2011**, *21*, 1700–1703.
50. Holst, J. R.; Stöckel, E.; Adams, D. J.; Cooper, A. I. High Surface Area Networks from Tetrahedral Monomers: Metal-Catalyzed Coupling, Thermal Polymerization, and "Click" Chemistry. *Macromolecules* **2010**, *43*, 8531–8538.
51. Plietzsch, O.; Schilling, C. I.; Grab, T.; Grage, S. L.; Ulrich, A. S.; Comotti, A.; Sozzani, P.; Muller, T.; Brase, S. Click Chemistry Produces Hyper-Cross-Linked Polymers with Tetrahedral Cores. *New J. Chem.* **2011**, *35*, 1577–1581.
52. Xie, L. H.; Suh, M. P. High CO_2-Capture Ability of a Porous Organic Polymer Bifunctionalized with Carboxy and Triazole Groups. *Chem.—Eur. J.* **2013**, *19*, 11590–11597.
53. Li, L.; Chen, Z.; Zhong, H.; Wang, R. Urea-Based Porous Organic Frameworks: Effective Supports for Catalysis in Neat Water. *Chem.—Eur. J.* **2014**, *20*, 3050–3060.
54. Li, L. Y.; Wang, J. Y.; Zhou, C. S.; Wang, R. H.; Hong, M. C. pH-Responsive Chelating N-Heterocyclic Dicarbene Palladium(II) Complexes: Recoverable Precatalysts for Suzuki-Miyaura Reaction in Pure Water. *Green Chem.* **2011**, *13*, 2071–2077.
55. Devadoss, A.; Chidsey, C. E. Azide-Modified Graphitic Surfaces for Covalent Attachment of Alkyne-Terminated Molecules by "Click" Chemistry. *J. Am. Chem. Soc.* **2007**, *129*, 5370–5371.
56. Bebensee, F.; Bombis, C.; Vadapoo, S. R.; Cramer, J. R.; Besenbacher, F.; Gothelf, K. V.; Linderoth, T. R. On-Surface Azide-Alkyne Cycloaddition on Cu(111): Does It "Click" in Ultrahigh Vacuum? *J. Am. Chem. Soc.* **2013**, *135*, 2136–2139.
57. Guan, B.; Ciampi, S.; Le Saux, G.; Gaus, K.; Reece, P. J.; Gooding, J. J. Different Functionalization of the Internal and External Surfaces in Mesoporous Materials for Biosensing Applications Using "Click" Chemistry. *Langmuir* **2011**, *27*, 328–334.
58. Chun, J.; Kang, S.; Kang, N.; Lee, S. M.; Kim, H. J.; Son, S. U. Microporous Organic Networks Bearing Metal-Salen Species for Mild CO_2 Fixation to Cyclic Carbonates. *J. Mater. Chem. A* **2013**, *1*, 5517–5523.
59. Ben, T.; Pei, C.; Zhang, D.; Xu, J.; Deng, F.; Jing, X.; Qiu, S. Gas Storage in Porous Aromatic Frameworks (PAFs). *Energy Environ. Sci.* **2011**, *4*, 3991–3999.
60. Weber, J.; Schmidt, J.; Thomas, A.; Bohlmann, W. Micropore Analysis of Polymer Networks by Gas Sorption and 129Xe NMR Spectroscopy: Toward a Better Understanding of Intrinsic Microporosity. *Langmuir* **2010**, *26*, 15650–15656.
61. Dawson, R.; Laybourn, A.; Clowes, R.; Khimyak, Y. Z.; Adams, D. J.; Cooper, A. I. Functionalized Conjugated Microporous Polymers. *Macromolecules* **2009**, *42*, 8809–8816.
62. Liang, Q.; Liu, J.; Wei, Y.; Zhao, Z.; MacLachlan, M. J. Palladium Nanoparticles Supported on a Triptycene-Based Microporous Polymer: Highly Active Catalysts for CO Oxidation. *Chem. Commun.* **2013**, *49*, 8928–8930.
63. Yuan, B.; Pan, Y.; Li, Y.; Yin, B.; Jiang, H. A Highly Active Heterogeneous Palladium Catalyst for the Suzuki-Miyaura and Ullmann Coupling Reactions of Aryl Chlorides in Aqueous Media. *Angew. Chem., Int. Ed.* **2010**, *49*, 4054–4058.
64. Martis, M.; Mori, K.; Fujiwara, K.; Ahn, W.-S.; Yamashita, H. Amine-Functionalized MIL-125 with Imbedded Palladium Nanoparticles as an Efficient Catalyst for Dehydrogenation of Formic Acid at Ambient Temperature. *J. Phys. Chem. C* **2013**, *117*, 22805–22810.
65. Radkevich, V. Z.; Senko, T. L.; Wilson, K.; Grishenko, L. M.; Zaderko, A. N.; Diyuk, V. Y. The Influence of Surface Functionalization of Activated Carbon on Palladium Dispersion and Catalytic Activity in Hydrogen Oxidation. *Appl. Catal. A: Gen.* **2008**, *335*, 241–251.
66. Huang, Y.; Liu, S.; Lin, Z.; Li, W.; Li, X.; Cao, R. Facile Synthesis of Palladium Nanoparticles Encapsulated in Amine-Functionalized Mesoporous Metal-Organic Frameworks and Catalytic for Dehalogenation of Aryl Chlorides. *J. Catal.* **2012**, *292*, 111–117.
67. Yuan, S.; Kirklin, S.; Dorney, B.; Liu, D.; Yu, L. Nanoporous Polymers Containing Stereocontorted Cores for Hydrogen Storage. *Macromolecules* **2009**, *42*, 1554–1559.
68. Leininger, S.; Stang, P. J.; Huang, S. P. Synthesis and Characterization of Organoplatinum Dendrimers with

1,3,5-Triethynylbenzene Building Blocks. *Organometallics* **1998**, *17*, 3981–3987.
69. Frisch, M. J.; Trucks, G. W.; Schlegel, H. B.; Scuseria, G. E.; Robb, M. A.; Cheeseman, J. R.; Montgomery, J. A., Jr.; Vreven, T.; Kudin, K. N.; Burant, J. C.; *et al*. *Gaussian 03*, Revision D.02; Gaussian, Inc.: Wallingford, CT, 2004.